Restoring self-limited growth of single-layer graphene on copper foil *via* backside coating

Nicolas Reckinger,[1,*] Marcello Casa,[2] Jeroen E. Scheerder,[3] Wout Keijers,[3] Matthieu Paillet,[4] Jean-Roch Huntzinger,[4] Emile Haye,[1] Alexandre Felten,[5] Joris Van de Vondel,[3] Maria Sarno,[2] Luc Henrard,[1] and Jean-François Colomer[1]

[1]Department of Physics, University of Namur, Rue de Bruxelles 61, 5000 Namur, Belgium.

[2] Department of Industrial Engineering and Centre NANO_MATES, University of Salerno Narrando Srl, Via Giovanni Paolo II, 132, 84084 Fisciano, Italy.

[3]Department of Physics and Astronomy, Celestijnenlaan 200D, KU Leuven, Leuven B-3001, Belgium.

[4]Laboratoire Charles Coulomb (L2C), Université de Montpellier, CNRS, Montpellier, France.

[5]SIAM platform, University of Namur, Rue de Bruxelles 61, 5000 Namur, Belgium.

†Electronic supplementary information (ESI) available.

Email: nicolas.reckinger@gmail.com

Abstract

The growth of single-layer graphene (SLG) by chemical vapor deposition (CVD) on copper surfaces is very popular because of the self-limiting effect that, in principle, prevents the growth of few-layer graphene (FLG). However, the reproducibility of the CVD growth of homogeneous SLG remains a major challenge, especially if one wants to avoid heavy surface treatments, monocrystalline substrates and expensive equipment to control the atmosphere inside the growth system. We demonstrate here that backside tungsten coating of copper foils allows for the exclusive growth of SLG with full coverage by atmospheric pressure CVD implemented in a vacuum-free furnace. We show that the absence of FLG patches is related to the absence of decomposition of methane on the backside and consequently to the suppression of C diffusion through copper. In the perspective of large-scale production of graphene, this approach constitutes a significant improvement to the traditional CVD growth process since (1) a tight control of the hydrocarbon flow is no longer required to avoid FLG formation and, consequently, (2) the growth duration necessary to reach full coverage can be drastically shortened.

Introduction

Chemical vapor deposition (CVD) has become the most popular production method of graphene, mainly because it holds great promises for industrial-scale applications. Catalytic CVD is a conceptually simple technique: it involves the decomposition of hydrocarbon precursors on substrates at high temperature in a controlled atmosphere at low[1] or atmospheric pressure.[2] In particular, copper (Cu) is extensively chosen as a substrate because it allows self-limited graphene growth due to its very low carbon (C) solubility, leading to highly homogeneous graphene sheets.[1]

The main focus of the recent research devoted to CVD growth of graphene is to produce ever larger graphene single crystals aiming, notably, to eliminate the detrimental effect of graphene domain boundaries on electron transport. The dominant approach towards this goal is to decrease the nucleation density of graphene by suppressing or passivating the nucleation sites (defects and surface steps at Cu's surface, impurities, etc.) by various treatments: chemical mechanical polishing;[3] electropolishing (EP);[4] prolonged thermal annealing;[5] high-pressure thermal annealing;[6] melting and resolidification;[7] pre-growth superficial oxidation;[8,9,10,11,12,13,14,15,16] surface engineering with melamine;[17] oxygen-assisted growth;[18] second passivation[19] and oxygen-assisted C contamination scavenging.[20] A second, less popular technique is to grow the graphene flakes in epitaxial registry with a monocrystalline Cu substrate. In consequence, the domains are aligned relatively to each other and merge seamlessly to produce graphene sheets in theory free of domain boundaries. Such monocrystalline substrates can be obtained from the epitaxial deposition of thin Cu films on various kinds of single crystals.[21,22,23,24,25] However, it is more convenient and cost-effective to start from cold-rolled polycrystalline Cu foils and convert them (at the surface or in the bulk) into monocrystals by appropriate strategies such as a prolonged thermal annealing at high temperature,[26,27] successive oxidative and reductive annealing at high temperature,[28,29] the hole-pocket method[30], or a Czochralski-like reconstruction induced through a temperature gradient.[31] A completely different route consists of working with the smooth surface of melted Cu.[32]

A very important challenge is related to the unwanted formation of few-layer graphene (FLG) domains inside the large-sized single-layer graphene (SLG) flakes or films. Even though SLG CVD growth on Cu is in principle self-limited, the presence of impurities or defects acting as nucleation centers breaks down this behavior[3], more specifically in atmospheric pressure conditions. The C-rich molecules that decompose on the frontside Cu surface are often regarded as the source for the FLG nucleation.[33] FLG flakes are considered to grow either on top of the first graphene layer, via layer-by-layer epitaxy,[34,35] or underneath, by C intercalation under the first-grown graphene flakes.[36,37] In that respect, C diffusion through the Cu foil is often disregarded as a supplier of carbonaceous species. However, Fang et al.[38] show that, despite C's low solubility in Cu, it can decompose on one face of a Cu enclosure, dissolve in and diffuse through Cu to form FLG flakes under graphene grown on the opposite side. Later, the same group claim that a tungsten (W) foil inserted inside the Cu enclosure can be used as a C sink to inhibit FLG growth.[39] By growing a thin Cu oxide layer on the backside of Cu foils prior to

graphene growth, Braeuninger-Weimer et al.[20] also demonstrate how oxygen (O) can diffuse through the Cu foil to scavenge C impurities, thereby enabling a drastic decrease of the graphene nucleation density on the front surface. Recent publications also evidence the complete suppression of FLG patches when a nickel (Ni) substrate (foil or foam) is placed between the fused silica carrier and the flat Cu foil.[40,41] In both cases, Ni acts as a C "getterer" and prevents C diffusion. Finally, Yoo et al.[42] deposit a thin layer of Ni on the Cu foil's backside. They find out that the graphene layer number grown on the frontside depends on the thickness of the Ni thin film.

In this work, we propose backside W deposition to obtain CVD growth of strictly homogeneous SLG films under atmospheric pressure with vacuum-free equipment. The main novelty of this study is the deposition of a thin W layer on the backside of electropolished Cu foils. We show that this W backside coating leads to the reproducible growth of exclusively SLG films. This remarkable result is explained by the complete suppression of C diffusion through the Cu foil, which restores self-limited growth of SLG. The W back coating enables to relax the strict control on the growth conditions, greatly facilitating the production of exclusively SLG sheets at an industrial scale.

Experimental

Pre-growth Cu foil treatment

We use a single 30×30 cm^2 Alfa Aesar (AA) Cu foil (reference number #46365: 25 μm-thick, purity 99.8%, annealed, uncoated) for all the CVD growth experiments, from which we either cut 2×8 cm^2 pieces if subjected to EP or 1×1 cm^2 pieces otherwise. The Cu pieces are sonicated, maintained in a vertical position, in a mixture of 60 ml of deionized water (DIW) and 2 ml of glacial acetic acid for 5 min, then rinsed in DIW for 2 min still in vertical position, rinsed in isopropanol for 2 min, and finally blow-dried with nitrogen.

Before EP, the Cu pieces are cleaned in the same way as described above. EP is performed by reproducing the experimental setup and conditions proposed in Ref. [12], with some adaptations. More specifically, we use a Coplin staining jar as a container. The Cu foil, fixed to a glass slide for easy handling (the grooves in the Coplin jar exactly match the size of the glass slide), is used as an anode and a *circa* 1-mm-thick Cu plate (of the same size as the Cu foil) is used as a cathode. Both electrodes are connected to the power supply using crocodile clips. It is important that the Cu foil is flat and parallel to the thicker Cu electrode to achieve reproducible, uniform EP. A constant voltage of 7 V is applied between the two electrodes for 60 s (inter-electrode distance: ~5 cm). The electrolyte solution is a mixture of 25 ml of DIW, 12.5 ml of phosphoric acid, 12.5 ml of ethanol, 2.5 ml of isopropanol, and 0.4 g of urea [12]. After EP, the Cu foil on the glass slide is transferred for rinsing to a second Coplin jar containing DIW, and sonicated for 2 min. Finally, it is stored in ethanol.

Graphene growth

The samples are first laid on a flat fused silica boat and inserted into a tubular fused silica reactor at room temperature. An Ar flow of 2000 sccm is admitted for 15 min in the tube after sealing (purge step). Meanwhile, the hotwall furnace is pre-heated to 1050 °C. Next, the fused silica tube is introduced into the furnace and the Ar flow is reduced to 500 sccm. The sample is then exposed to Ar alone during 15 min and is mildly oxidized at the surface due to residual oxidizing impurities. Thereafter, the Cu foil's surface is reduced for 45 min with the addition of 20 sccm of H_2. Afterwards, dilute methane (CH_4; 5% in 95% of Ar) is injected to grow graphene. For all the W-free samples, the dilute CH_4 flow is set to 0.5 sccm, while it is variable for the W-capped ones (with a maximum of 3 sccm). The reactor is extracted 1 h later from the furnace after graphene growth and left to cool down naturally in the same gas mixture. The conditions corresponding to a dilute CH_4 flow of 0.5 sccm and a growth duration of 1 h are referred to as the "standard growth conditions". During the whole growth procedure, the reactor is maintained at atmospheric pressure (no pumping equipment connected to the system, which is called "vacuum-free"). For more details, we refer the reader to our previous publication.[28]

Graphene transfer

Graphene is transferred onto silicon dioxide/silicon (SiO_2/Si) substrates by the widely used wet, polymer-assisted method. After poly(methyl methacrylate) (PMMA) coating and baking at 110 °C, Cu is etched in an ammonium persulfate solution. The PMMA/graphene stack is next rinsed thoroughly in DIW and fished on the SiO_2/Si support. The sample is left to dry overnight, baked at 120 °C for 1 h, and, finally, PMMA is stripped with acetone. Both the W-free and W-coated samples are transferred in this way.

W deposition

W (50 nm; 99.95% purity) is coated on the backside of the Cu pieces by magnetron sputtering with a deposition pressure of 10^{-2} mbar (base pressure = 10^{-4} mbar) and Ar as sputtering gas. The deposited thickness is controlled by a quartz balance next to the sample.

More details about the experimental techniques (scanning electron microscopy, energy-dispersive X-ray spectroscopy, X-ray photoelectron spectroscopy, Raman spectroscopy setup, X-ray diffraction, Hall bar fabrication, transport measurements) can be found in the ESI.

Results and discussion

To prevent any CH_4 diffusion through Cu, we deposit a thin (50 nm) W layer on the backside of electropolished Cu pieces (see the ESI, Figs. S1−9, for a critical review of various procedures and investigations carried out to solve and understand the origin of persistent reproducibility issues in terms of coverage and uniformity). Contrary to the use of foils or foams as a support

for Cu samples (see Fig. S9), deposition ensures an intimate contact with the Cu foil's backside. In addition, the Cu specimens remain flat, facilitating the manipulation (as opposed to the Cu enclosure configuration). Since W has a very high melting point (as high as 3422 °C at ambient pressure), the thin film is able to sustain the harsh thermal conditions in the reactor and retain its integrity during the full procedure. We choose W as a backside coating material instead of Ni because it is known to absorb and release carbon during thermal treatments[42]. W is more appropriate as a C diffusion barrier because it is able to form a carbidic compound with a high thermal stability.[43]

In Fig. 1a, a low-magnification scanning electron microscopy image of the surface of a Cu piece after graphene growth (standard growth conditions) with W covering half of the backside (this half is called the "W half" in the following) is shown. Spectacularly enough, the two halves of the Cu foil exhibit very distinct morphological aspects. The left side (W half) of Fig. 1a is very heterogeneously contrasted, meaning that Cu remains polycrystalline. The other half reveals a homogeneous morphology, indicative of a Cu reconstruction in the (111) crystalline orientation.[28] The reconstruction of cold-rolled Cu foils occurs at high temperature, via the mechanism of abnormal grain growth, if the grain boundaries are left free to evolve.[28] In the presence of a W coating over the underside of Cu foils, the Cu grain boundaries are pinned and any further reconstruction is prevented even at temperatures as high as 1050 °C.

It is also worth noting that the graphene flakes on the W-free half are hexagonal, while they exhibit an irregular shape on the other half, probably related to the polycrystallinity of Cu. More importantly, on the W-free half, FLG islands are clearly visible. In contrast, it is difficult to assess the presence of FLG flakes on the W half due to the mosaic of Cu grain orientations. In addition, the density in SLG graphene flakes is significantly lower on the W half, suggesting that W plays a crucial role in the supply of C building blocks to the front surface.

To increase the graphene coverage on the W half and to better visualize the FLG flakes, we produce a similar sample with a slightly higher dilute CH_4 flow (0.6 sccm) and we transfer it on a 90-nm-thick SiO_2/Si sample (see Fig. 1b). Spectacularly, the W half is completely devoid of FLG graphene islands, while the other half is completely scattered with them. To quantitatively confirm this observation, simultaneous micro-Raman and micro-reflection analyses are performed on the whole sample. Fig. 1c displays the number of layers N_G deduced from the normalized Raman G-band area. Further characterization and analysis of this sample are available in the ESI (see Figs. S10−12). It gives a definitive proof that the W half of the sample comprises almost uniquely SLG while the W-free half is very heterogeneous. We evaluate the quality of the present graphene film by the defect-related D band. The average spectrum corresponding to Fig. 1c is presented in Fig. S11. It is very comparable (very weak D band) to the quality obtained from graphene grown on Cu foils without W layer on the backside.[28]

Consequently, in all the following experiments, since the W layer pins the Cu grain boundaries, we first (1) reconstruct the Cu foil in the unique (111) orientation after EP, (2) then only deposit W on the backside, and (3) finally, grow graphene on the frontside of the Cu foil. In this way, we can combine the benefits of the monocrystalline Cu foil and of the underside W coating to

grow purely monolayer, monocrystalline, FLG-free graphene sheets in a single time. Fig. 1d displays a photograph of four such samples after growth and heating on a hot plate in air at 150 °C for 5 min, corresponding to a progressive increase of the dilute CH_4 flow (from 0.6 to 1.2 sccm by steps of 0.2 sccm). We can clearly see that the graphene coverage increases progressively, until it is complete for 1.2 sccm (the reddish color indicates oxidized Cu). Fig. 1e shows an X-ray diffraction (XRD) spectrum of a Cu sample with a W backside coating (deposited after Cu reconstruction) after graphene growth. The very intense, unique Cu(111) peak confirms the Cu monocrystallization (except for a few residual (200) grains[26,28]). Finally, Fig. 1f reveals an optical microscopy image of typical submillimeter monolayer graphene flakes grown on the same type of W-coated Cu(111) substrate.
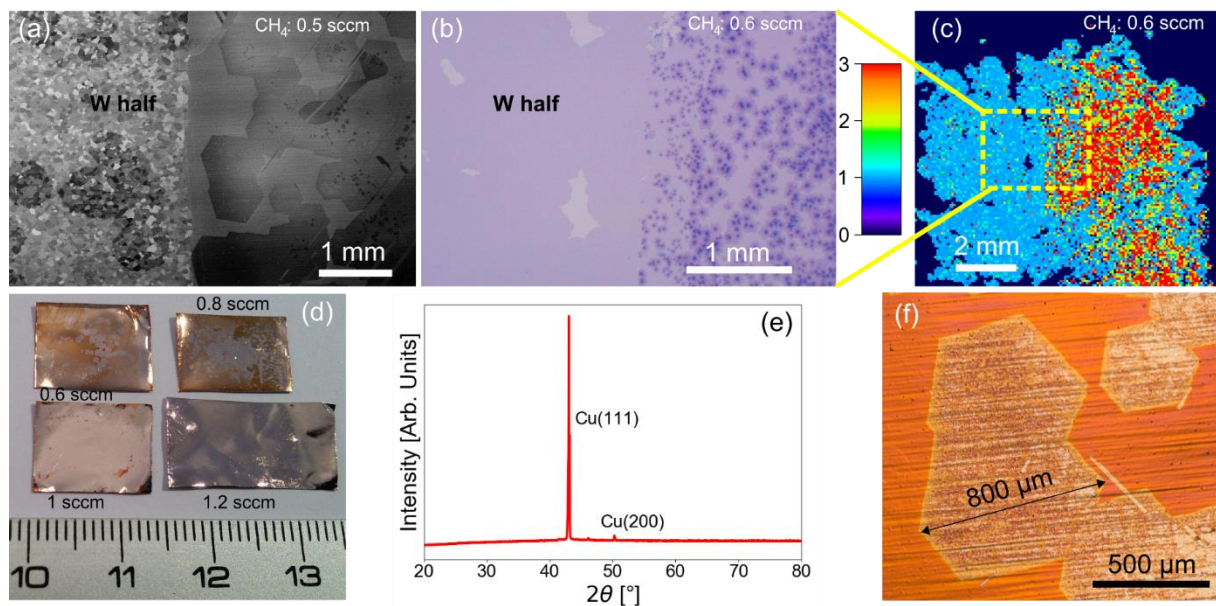

Fig. 1: (a) Low-magnification scanning electron microscopy image of a Cu piece after graphene growth with a 50-nm-thick W layer covering the left half of its backside (grown with a 0.5 sccm dilute CH_4 flow). (b) Optical microscopy picture of a graphene sample (grown with a 0.6 sccm dilute CH_4 flow on the same type of Cu sample as described in (a)) transferred onto a 90-nm-thick silicon dioxide/silicon substrate. (c) Map of the number of layers of the sample shown in (b) deduced from the normalized integrated Raman G-band intensity. The dashed white rectangle corresponds to the region shown in (b). (d) Four Cu samples (W backside deposition after Cu(111) reconstruction) corresponding to a progressive increase of the dilute CH_4 flow (from 0.6 to 1.2 sccm by steps of 0.2 sccm), photographed after graphene growth and heating on a hot plate in air to reveal the oxidized, uncovered (reddish) Cu surface. (e) X-ray diffraction spectrum of a Cu(111) sample with a W backside coating (deposited after Cu reconstruction) after graphene growth. (f) Optical microscopy picture of typical hexagonal graphene domains grown on a W-coated Cu(111) sample.

Next, we perform simultaneous micro-reflection and micro-Raman mapping on the 1.2 sccm sample of Fig. 1d transferred onto a 90-nm-thick SiO_2/Si substrate (see also the ESI, Figs. S13−15) to give a quantitative support to our claim of an exclusively SLG film. We follow the approach detailed in Ref. [44], with N_G the number of layers obtained using the normalized Raman G-band area, and N_{OC} the number of layers obtained from the laser optical contrast (see

Fig. 2a and b). Both data sets agree and confirm that except for two edges, the sample is almost exclusively composed of SLG. Furthermore, in Fig. 2c, the 3-dimensional bivariate histograms of N_G and N_{OC}, as well as the histograms for each independent quantity, are displayed for the central part of the sample delimited by the yellow dashed frame in Fig. 2a. Quantitatively, on the 6500 points where the number of layers could be attributed, 3.1% correspond to the bare substrate (*i.e.* no graphene), 1.1% are 0−1 layer (only partial graphene coverage), 94.2% are SLG, 1.3% are between 1 and 2 layers (graphene wrinkles, partial bilayer graphene coverage, etc.) and 0.3% is bilayer (mostly small graphene pieces scratched and folded during the transfer).
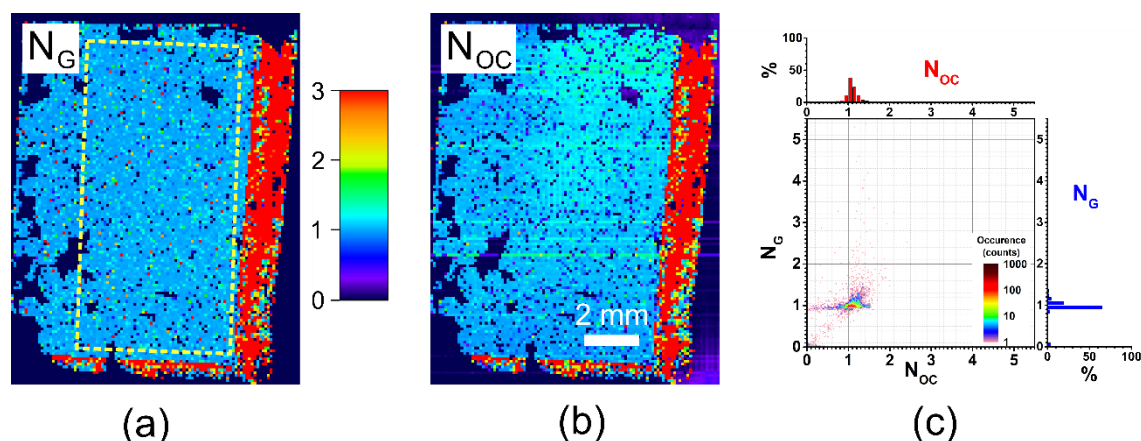

Fig. 2: Maps of the number of layers of the sample grown with a 1.2 sccm dilute CH_4 flow and transferred on a 90-nm-thick silicon dioxide/silicon substrate (a) N_G, the number of layers deduced from the normalized integrated Raman G-band intensity and (b) N_{OC}, the number of layers deduced from the laser optical contrast. (c) 3D bivariate histogram (0.025 bin size) of N_{OC} and N_G derived from the maps (a) and (b). The region considered is delimited by the dashed yellow frame shown in (a). The number of occurrences (frequency counts) is color-coded as shown on the graphs. On top (resp. right hand side) are displayed the corresponding histograms of N_{OC} (resp. N_G).

We also evaluate the W backside coating method when the CH_4 flow is significantly increased (3 sccm, maximal value of our mass flow), with the objective of drastically decreasing the growth duration (fixed here to 5 min, instead of 1 h as before). The corresponding data are given in the ESI, Figs. S16−18. The Raman spectroscopy/optical contrast mapping results show that the corresponding graphene is also exclusively monolayer, with an almost complete coverage, evidencing the robustness of the synthesis technique. This is a very important aspect of the W backside coating approach in the perspective of industrial production since a tight control of the CH_4 flow is no longer required to avoid FLG formation and the full-coverage synthesis process duration can be dramatically shortened. The efficiency of the W backside coating to prevent FLG growth confirms the hypothesis that FLG islands grow under the first SLG layer. Consequently, after full graphene coverage, there is no more catalytic surface available for CH_4 decomposition into carbon building blocks and graphene stops growing (the "self-limited" growth mechanism). A further exposure to CH_4 will then not lead to FLG growth.

To better understand the precise role of the W coating, we inspect, by depth profile X-ray photoelectron spectroscopy (XPS) (Fig. 3a and b) and XRD (Fig. 3c), the chemical and morphological evolution of a W film just after deposition (no thermal treatment) on Cu and after graphene growth, respectively. The XPS analysis shows that the as-deposited W layer is slightly oxidized (Fig. 3a) and contains no C (within the detection threshold of XPS of < 0.5 at% for the acquisition parameters used during the XPS profile). After graphene growth, Cu and W appear intermixed (roughly a 50% Cu / 50% W alloy) and again, no C is contained in that layer, in agreement with Fang *et al.*[39] It is true that graphene can be grown on W foils[43] but, here, C detected at the very surface of the sample corresponds to organic contamination. Furthermore, from Fig. 3c, the as-deposited W film appears amorphous, since no W-related diffraction peak can be observed. The graphene growth process leads to the crystallization of metallic W, in the cubic $I_{m\bar{3}m}$ structure (space group 229), with the occurrence of diffraction peaks located at 40.3, 58.2, 73.2, 87, and 100.6° attributed to the (110), (200), (211), (220) and (310) crystallographic orientations, respectively.[45] W is known for its carbide forming capabilities[43] but we find no trace of diffraction peaks related to W carbide. Based on these two analyses, it appears that the W layer acts as a C diffusion barrier rather than as a C sink, since no C appears to be trapped inside the W-bearing layer. We illustrate the proposed working principle in Fig. 3d.

It is worth discussing here in more details the role of the W backside coating. The W foil in reference [39] is placed inside a Cu enclosure, and the authors claim it to act as a carbon sink, while in our case the W layer is rather used as a barrier for carbon diffusion (as confirmed above by XRD and XPS). The two observations are not incompatible, and are related to the different role played by W in the "Cu enclosure + W foil" configuration versus "W-coated flat Cu foil" configuration. In our configuration, the W layer is in intimate contact with Cu, preventing the decomposition of CH_4 on the backside and the diffusion of C through the Cu foil. In consequence, FLG islands do not grow at all on the top surface. This is in stark contrast with the case of reference [39], where FLG inclusions are formed in the first stages of the growth, and claimed to be progressively removed after more than 30 min of process by the W foil inside the Cu enclosure.
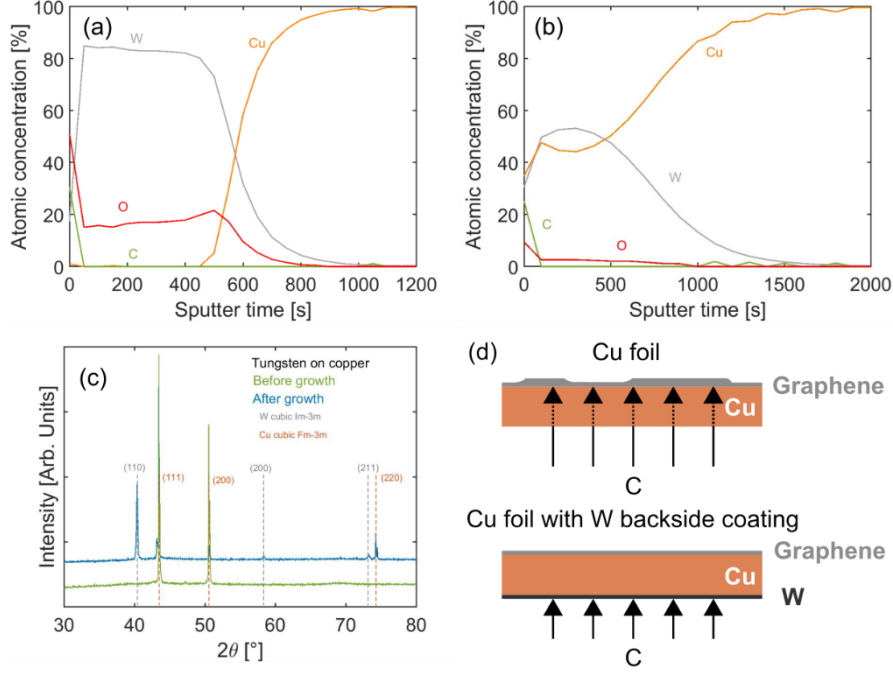
Fig. 3: X-ray photoelectron spectroscopy depth profile of a W film on Cu (a) before (as-deposited) and (b) after graphene growth. (c) X-ray diffraction analysis of a W film on Cu, just after deposition and after graphene growth. (d) Working principle.

Finally, electronic characterization of the as-synthesized graphene (transferred on a 300-nm-thick SiO_2/p^{++} Si substrate) is carried out using a graphene field-effect transistor (GFET) in a Hall bar configuration to evaluate its quality (see Fig. S19a). Measurements of the longitudinal resistivity $\rho_{xx} = V_{xx}/I \times W/L$ and transversal (Hall) resistivity $\rho_{xy} = V_{xy}/I$ are conducted with a current bias of 10 μA (see Fig. S19b). By sweeping a gate voltage V_G, applied between the graphene Hall bar and the p^{++} Si electrode, the Fermi level of graphene can be altered, resulting in the well-known ambipolar field-effect behavior. The sheet conductance $\sigma_{xx} = 1/\rho_{xx}$ versus V_G for a representative GFET is shown in Fig. 4a, at room temperature and at 400 mK. In the insets, the electronic level filling of the Dirac cone is schematically indicated by the blue regions. We find an average electron-hole mobility at both temperatures of ~4×10^3 cm^2/(Vs). This value is close to the value previously found for graphene grown on Cu foils without the W backside coating (with an average electron-hole mobility of ~5×10^3 cm^2/(Vs)),[46] within the experimental and process-to-process variability. Hall measurements are performed at 400 mK, at a magnetic field of 5 T applied perpendicular to the graphene plane. The Hall conductivity as a function of V_G, shown in Fig. 4b, demonstrates the clear half-integer quantum Hall effect, $\sigma_{xy} = 4e^2/h \times (n + 1/2)$ (n = 0, 1, 2,…). Green vertical lines exhibit the gate values where the first derivative of σ_{xy} has local minima (shown in the inset to Fig. 4b), aiding in the identification of the plateaus This is typical of SLG[47,48] and serves as an indication of the high electronic quality of the sample.[49]
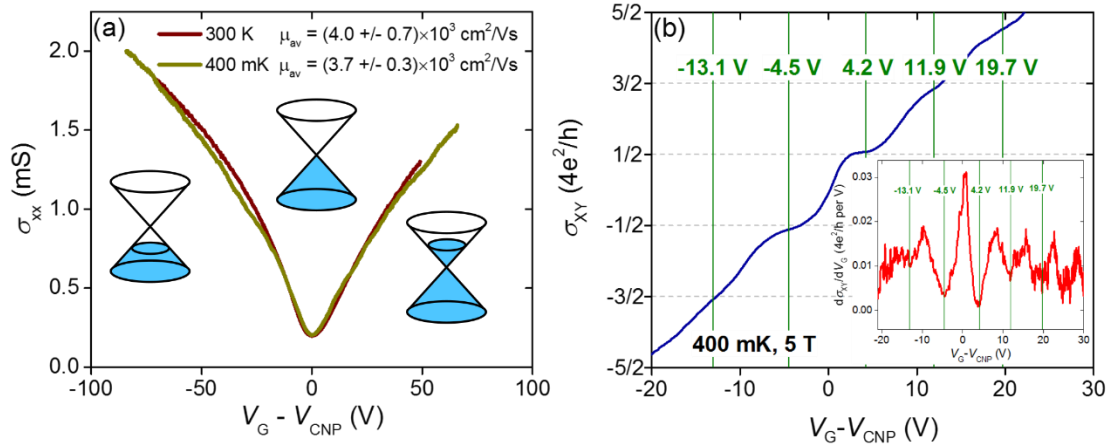
Fig. 4: (a) Graphene sheet conductivity as a function of the gate voltage with respect to the charge neutrality point, $\sigma_{xx}(V_G - V_{CNP})$, at room temperature and 400 mK. The insets portray the dispersion bands of graphene, with the blue areas representing the level filling. (b) Hall conductivity $\sigma_{xy}(V_G - V_{CNP})$ at $B = 5$ T and 400 mK. Plateaus appear at $\sigma_{xy} = 4e^2/h \times (n + 1/2)$, with n an integer. Inset: first derivative of σ_{xy}.

Conclusion

We demonstrate that the reproducible growth of exclusively SLG in vacuum-free equipment is achieved by coating a thin W layer on the backside of Cu foils. The W layer completely blocks C diffusion from the backside towards the front surface of the foil. These results substantiate that this C diffusion through the Cu foil (and not the morphology of the upper Cu surface) is the determining factor in the growth of FLG inclusions. Therefore, the tight control over the hydrocarbon flow usually needed during the CVD protocol to achieve purely SLG with full coverage can be relaxed. At the same time, the possibility of increasing the hydrocarbon flow enables the drastic diminution of the growth procedure duration. That leeway on the growth conditions (both in terms of hydrocarbon flow and growth duration) constitutes a major contribution in the perspective of industrializing the SLG production.

Acknowledgement

N.R. conceived the experiment, analyzed all the results, and wrote the initial version of the manuscript. N.R. executed the graphene CVD growths and transfers, and carried out the SEM and optical imaging. M.C. performed the pre-growth copper foil electropolishing, collaborated on graphene growth and optical imaging. J.E.S., W.K. and J.V.d.V. fabricated the graphene FET devices, conducted, and analyzed the electronic transport measurements. M.P. et J.-R.H. realized the Raman spectroscopy and optical contrast characterization, treated, and analyzed the results. E.H. performed the XRD analysis and interpreted the results. A.F. carried out the XPS analysis and analyzed the data. M.S. brought her expertise in CVD growth of nanocarbons. L.H. supervised the project. All authors participated to the redaction and commented on the manuscript.

References

[1] X. Li, W. Cai, J. An, S. Kim, J. Nah, D. Yang, R. Piner, A. Velamakanni, I. Jung, E. Tutuc, S. K. Banerjee, L. Colombo and R. S. Ruoff, *Science*, 2009, **324**, 1312.

[2] I. Vlassiouk, M. Regmi, P. Fulvio, S. Dai, P. Datskos, G. Eres and S. Smirnov, *ACS Nano*, 2011, **5**, 6069.

[3] G. H. Han, F. Güneş, J. J. Bae, E. S. Kim, S. J. Chae, H.-J. Shin, J.-Y. Choi, D. Pribat and Y. H. Lee, *Nano Lett.*, 2011, **11**, 4144.

[4] Z. Luo, Y. Lu, D. W. Singer, M. E. Berck, L. A. Somers, B. R. Goldsmith and A. T. C. Johnson, *Chem. Mater.*, 2011, **23**, 1441.

[5] H. Wang, G. Wang, P. Bao, S. Yang, W. Zhu, X. Xie and W.-J. Zhang, *J. Am. Chem. Soc.*, 2012, **134**, 3627.

[6] Z. Yan, J. Lin, Z. Peng, Z. Sun, Y. Zhu, L. Li, C. Xiang, E. L. Samuel, C. Kittrell and J. M. Tour, *ACS Nano*, 2012, **6**, 9110.

[7] A. Mohsin, L. Liu, P. Liu, W. Deng, I. N. Ivanov, G. Li, O. E. Dyck, G. Duscher, J. R. Dunlap, K. Xiao and G. Gu, *ACS Nano*, 2013, **7**, 8924.

[8] Y. Hao, M. S. Bharathi, L. Wang, Y. Liu, H. Chen, S. Nie, X. Wang, H. Chou, C. Tan, B. Fallahazad, H. Ramanarayan, C. W. Magnuson, E. Tutuc, B. I. Yakobson, K. F. McCarty, Y.-W. Zhang, P. Kim, J. Hone, L. Colombo and R. S. Ruoff, *Science*, 2013, **342**, 720.

[9] L. Gan and Z. Luo, *ACS Nano*, 2013, **7**, 9480.

[10] H. Zhou, W. J. Yu, L. Liu, R. Cheng, Y. Chen, X. Huang, Y. Liu, Y. Wang, Y. Huang and X. Duan, *Nat. Commun.*, 2013, **4**, 3096.

[11] G. Eres, M. Regmi, C. M. Rouleau, J. Chen, I. N. Ivanov, A. A. Puretzky and D. B. Geohegan, *ACS Nano*, 2014, **8**, 5657.

[12] V. Miseikis, D. Convertino, N. Mishra, M. Gemmi, T. Mashoff, S. Heun, N. Haghighian, F. Bisio, M. Canepa, V. Piazza and C. Coletti, *2D Mater.*, 2015, **2**, 014006.

[13] J. Li, X.-Y. Wang, X.-R. Liu, Z. Jin, D. Wang and L.-J. Wan, *J. Mater. Chem. C*, 2015, **3**, 3530.

[14] J. Kraus, M. Böbel and S. Günther, *Carbon*, 2016, **96**, 153.

[15] S. Wang, H. Hibino, S. Suzuki and H. Yamamoto, *Chem. Mater.*, 2016, **28**, 4893.

[16] P. H. Q. Pham, W. Zhou, N. V. Quach, J. Li, J.-G. Zheng and P. J. Burke, *Chem. Mater.*, 2016, **28**, 6511.

[17] L. Lin, J. Li, H. Ren, A. L. Koh, N. Kang, H. Peng, H. Q. Xu and Z. Liu, *ACS Nano*, 2016, **10**, 2922.

[18] W. Guo, F. Jing, J. Xiao, C. Zhou, Y. Lin and S. Wang, *Adv. Mater.*, 2016, **28**, 3152.

[19] L. Lin, L. Sun, J. Zhang, J. Sun, A. L. Koh, H. Peng and Z. Liu, *Adv. Mater.*, 2016, **28**, 4671.

[20] P. Braeuninger-Weimer, B. Brennan, A. J. Pollard and S. Hofmann, *Chem. Mater.*, 2016, **28**, 8905.

[21] D. L. Miller, M. W. Keller, J. M. Shaw, A. N. Chiaramonti and R. R. Keller, *J. Appl. Phys.*, 2012, **112**, 064317.

[22] Y. Ogawa, B. Hu, C. M. Orofeo, M. Tsuji, K. Ikeda, S. Mizuno, H. Hibino and H. Ago, *J. Phys. Chem. Lett.*, 2012, **3**, 219.

[23] R. M. Jacobberger and M. S. Arnold, *Chem. Mater.*, 2013, **25**, 871.

[24] H. Ago, Y. Ohta, H. Hibino, D. Yoshimura, R. Takizawa, Y. Uchida, M. Tsuji, T. Okajima, H. Mitani and S. Mizuno, *Chem. Mater.*, 2015, **27**, 5377.

[25] V. L. Nguyen, D. J. Perello, S. Lee, C. T. Nai, B. G. Shin, J.-G. Kim, H. Y. Park, H. Y. Jeong, J. Zhao, Q. A. Vu, S. H. Lee, K. P. Loh, S.-Y. Jeong and Y. H. Lee, *Adv. Mater.*, 2016, **28**, 8177.

[26] L. Brown, E. B. Lochocki, J. Avila, C.-J. Kim, Y. Ogawa, R. W. Havener, D.-K. Kim, E. J. Monkman, D. E. Shai, H. I. Wei, M. P. Levendorf, M. Asensio, K. M. Shen and J. Park, *Nano Lett.*, 2014, **14**, 5706.

[27] V. L. Nguyen, B. G. Shin, D. L. Duong, S. T. Kim, D. Perello, Y. J. Lim, Q. H. Yuan, F. Ding, H. Y. Jeong, H. S. Shin, S. M. Lee, S. H. Chae, Q. A. Vu, S. H. Lee and Y. H. Lee, *Adv. Mater.*, 2015, **27**, 1376.

[28] N. Reckinger, X. Tang, F. Joucken, L. Lajaunie, R. Arenal, E. Dubois, B. Hackens, L. Henrard and J.-F. Colomer, *Nanoscale*, 2016, **8**, 18751.

[29] H. Wang, X. Xu, J. Li, L. Lin, L. Sun, X. Sun, S. Zhao, C. Tan, C. Chen, W. Dang, H. Ren, J. Zhang, B. Deng, A. L. Koh, L. Liao, N. Kang, Y. Chen, H. Xu, F. Ding, K. Liu, H. Peng and Z. Liu, *Adv. Mater.*, 2016, **28**, 8968.

[30] H. D. Phan, J. Jung, Y. Kim, V. N. Huynh and C. Lee, *Nanoscale*, 2016, **8**, 13781.

[31] X. Xu, Z. Zhang, J. Dong, D. Yi, J. Niu, M. Wu, L. Lin, R. Yin, M. Li, J. Zhou, S. Wang, J. Sun, X. Duan, P. Gao, Y. Jiang, X. Wu, H. Peng, R. S. Ruoff, Z. Liu, D. Yu, E. Wang, F. Ding and K. Liu, *Sci. Bull.*, 2017, **62**, 1074.

[32] Y. A. Wu, Y. Fan, S. Speller, G. L. Creeth, J. T. Sadowski, K. He, A. W. Robertson, C. S. Allen and J. H. Warner, *ACS Nano*, 2012, **6**, 5010.

[33] H. Q. Ta, D. J. Perello, D. L. Duong, G. H. Han, S. Gorantla, V. L. Nguyen, A. Bachmatiuk, S. V. Rotkin, Y. H. Lee and M. H. Rümmeli, *Nano Lett.*, 2016, **16**, 6403.

[34] K. Yan, H. Peng, Y. Zhou, H. Li and Z. Liu, *Nano Lett.*, 2011, **11**, 1106.

[35] L. Liu, H. Zhou, R. Cheng, W. J. Yu, Y. Liu, Y. Chen, J. Shaw, X. Zhong, Y. Huang and X. Duan, *ACS Nano*, 2012, **6**, 8241.

[36] S. Nie, W. Wu, S. Xing, Q. Yu, J. Bao, S. Pei and K. F. McCarty, *New J. Phys.*, 2012, **14**, 093028.

[37] Q. Li, H. Chou, J.-H. Zhong, J.-Y. Liu, A. Dolocan, J. Zhang, Y. Zhou, R. S. Ruoff, S. Chen and W. Cai, *Nano Lett.*, 2013, **13**, 486.

[38] W. Fang, A. L. Hsu, Y. Song, A. G. Birdwell, M. Amani, M. Dubey, M. S. Dresselhaus, T. Palacios and J. Kong, *ACS Nano*, 2014, **8**, 6491.

[39] W. Fang, A. Hsu, Y. C. Shin, A. Liao, S. Huang, Y. Song, X. Ling, M. S. Dresselhaus, T. Palacios and J. Kong, *Nanoscale*, 2015, **7**, 4929.

[40] D. Ding, P. Solís-Fernández, H. Hibino and H. Ago, *ACS Nano*, 2016, **10**, 11196.

[41] I. H. Abidi, Y. Liu, J. Pan, A. Tyagi, M. Zhuang, Q. Zhang, A. A. Cagang, L.-T. Weng, P. Sheng, W. A. Goddard and Z. Luo, *Adv. Funct. Mater.*, 2017, **27**, 1700121.

[42] M. S. Yoo, H. C. Lee, S. Lee, S. B. Lee, N.-S. Lee and K. Cho, *Adv. Mater.*, 2017, **29**, 1700753.

[43] Z. Zou, L. Fu, X. Song, Y. Zhang and Z. Liu, *Nano Lett.*, 2014, **14**, 3832.

[44] M. Bayle, N. Reckinger, A. Felten, P. Landois, O. Lancry, B. Dutertre, J.-F. Colomer, A.-A. Zahab, L. Henrard, J.-L. Sauvajol and M. Paillet, *J. Raman Spectrosc.*, 2018, **49**, 36.

[45] R. W. G. Wyckoff, Crystal Structures; 2nd Edition.; Interscience Publishers, 1963.

[46] J. E. Scheerder, T. Picot, N. Reckinger, T. Sneyder, V. S. Zharinov, J.-F. Colomer, E. Janssens and J. Van de Vondel, *Nanoscale*, 2017, **9**, 10494.

[47] K. S. Novoselov, A. K. Geim, S. V. Morozov, D. Jiang, M. I. Katsnelson, I. V. Grigorieva, S. V. Dubonos and A. A. Firsov, *Nature*, 2005, **438**, 197.

[48] K. S. Novoselov, E. McCann, S. V. Morozov, V. I. Fal'ko, M. I. Katsnelson, U. Zeitler, D. Jiang, F. Schedin and A. K. Geim, *Nat. Phys.*, 2006, **2**, 177.

[49] Z. Jiang, Y. Zhang, Y.-W. Tan, H. L. Stormer and P. Kim, *Solid State Commun.*, 2007, **143**, 14.